Earthquakes and Structures, *Vol. 12, No. 6 (2017) 603-617*
DOI: https://doi.org/10.12989/eas.2017.12.6.603

Performance of hybrid beam-column joint cast with high strength concrete

M.A. Al-Osta[1a], A.M. Al-Khatib[1b], M.H. Baluch[1c], A.K. Azad[1d] and M.K. Rahman[*2]

[1]*Department of Civil Engineering, King Fahd University of Petroleum & Minerals (KFUPM), Dhahran 31261, Saudi Arabia*
[2]*Center for Engineering Research, Research Institute, King Fahd University of Petroleum & Minerals (KFUPM), Dhahran 31261, Saudi Arabia*

(Received October 3, 2016, Revised November 18, 2016, Accepted May 26, 2017)

Abstract. This paper presents investigation into the behavior of beam-column joints, with the joint region concrete being replaced by steel fiber reinforced concrete (SFRC) and by ultra-high performance concrete (UHPC). A total of ten beam-column joint specimens (BCJ) were tested experimentally to failure under monotonic and cyclic loading, with the beam section being subjected to flexural loading and the column to combined flexural and axial loading. The joint region essentially transferred shear and axial stresses as received from the column. Steel fiber reinforced concrete (SFRC) and ultra-high performance concrete (UHPC) were used as an innovative construction and/or strengthening scheme for some of the BCJ specimens. The reinforced concrete specimens were reinforced with longitudinal steel rebar, 18 mm, and some specimens were reinforced with an additional two ties in the joint region. The results showed that using SFRC and UHPC as a replacement concrete for the BCJ improved the joint shear strength and the load carrying capacity of the hybrid specimens. The mode of failure was also converted from a non-desirable joint shear failure to a preferred beam flexural failure. The effect of the ties in the SFRC and UHPC joint regions could not be observed due to the beam flexural failure. Several models were used in estimating the joint shear strength for different BCJ specimens. The results showed that the existing models yielded wide-ranging values. A new concept to take into account the influence of column axial load on the shear strength of beam-column joints is also presented, which demonstrates that the recommended values for concrete tensile strength for determination of joint shear strength need to be amended for joints subject to moderate to high axial loads. Furthermore, finite element model (FEM) simulation to predict the behaviour of the hybrid BCJ specimens was also carried out in an ABAQUS environment. The result of the FEM modelling showed good agreement with experimental results.

Keywords: beam-column joint; hybrid joint; steel fiber reinforced concrete; ultra high performance concrete; joint shear strength; finite element model

1. Introduction

Beam-column joints, one of the most common elements in buildings, are subjected to combined action of high shear and bending moment. The damage in the joints has been observed in recent destructive earthquakes in many countries around the world (Japan Earthquake 2010, Taiwan Earthquake 1999, Turkey Earthquake 1999). The beam-column joint (BCJ) in moment resisting frame structures designed according to earlier codes have insufficient shear reinforcement and development length. This was cited as the main cause of damage in the joint (Pampanin *et al*. 2002, Braga *et al*. 2009). The prevention of shear-induced damage of joints has given impetus to researchers to explore the use of strengthening materials or techniques at the joints. Pantelides *et al*. (2000) and Sasmal *et al*. (2010) used FRP laminates to improve the ductility and the load carrying capacity of BCJ specimens. El-Amoury *et al*. (2002) enhanced the ductility and load carrying capacity of the BCJ by retrofitting the specimens with GFRP. Karayannis *et al*. (2002) improved the load carrying capacity and the energy dissipated of BCJ specimens by retrofitting the specimens with thin reinforced concrete jacket. Alsayed *et al*. (2010) reported that the shear resistance, deformation capacity, and stiffness of BCJ specimens were improved by retrofitting the specimens with CFRP. Danish *et al*. (2013) presented a finite element simulation to capture the nonlinear response of a typical low strength beam-column joint by using the software DIANA.

The properties of steel fibre reinforced concrete mainly depend on the concrete mix, steel fibre content, fibre shape and bond characteristics. Steel fibers are used to enhance the ability of concrete to resist tensile forces. Song *et al*. (2004), Barros *et al*. (2008), El-Dieb *et al*. (2009), Shende *et al*. (2012) and Prem *et al*. (2012) improved the mechanical properties of different types of concrete by mixing the concrete with steel fiber. Using high strength

*Corresponding author, Associate Professor
E-mail: mkrahman@kfupm.edu.sa
[a]Assistant Professor
E-mail: malosta@kfupm.edu.sa
[b]Ph.D. Student
E-mail: g201205960@kfupm.edu.sa
[c]Professor
E-mail: mohsain.baluch@gmail.com
[d]Professor
E-mail: akazad1334@yahoo.com

ISSN: 2092-7614 (Print), 2092-7622 (Online)

concrete in strengthening reinforced concrete BCJ can enhance the shear capacity and the ductility of the joint. Literature review shows limited experimental studies have been conducted on BCJs strengthened with high strength concrete. Ganesan *et al*. (2007), Wang *et al*. (2007) and Sarsam *et al*. (2010) improved the ductility (large displacement with small cracks) of the BCJ by mixing concrete with steel fiber. Röhm *et al*. (2012) studied the behavior of the reinforced concrete BCJ strengthened with steel fiber reinforced concrete in the joint area under cyclic loading. It is found that the use of steel fiber in the joint shifted the cracks from the joint to the beam. Perumal *et al*. (2011) and Oinam *et al*. (2013) improved the stiffness, energy dissipation, and ductility of reinforced concrete (RC) exterior BCJs by strengthening the specimens with SFRC, and polypropylene fiber reinforced concrete. Ha *et al*. (2013) studied the performance of high strength reinforced concrete BCJ under cyclic loads. The load carrying capacity and the energy dissipation capacity of the specimens with high strength mortar in the joint region was higher than for the control specimens. Keerthana *et al*. (2014) investigated the behavior of hybrid fiber reinforced BCJs under cyclic loading. The results showed that the strength, stiffness, and energy dissipation for the BCJ specimens were improved. Chidambaram and Agarwal (2015) conducted an experimental work on six exterior BCJ with different concrete composites under cyclic loading. Three different types of fiber were used namely hooked end steel fiber; brass coated steel fiber and polypropylene fiber with hybrid cementitious composites (HCC). It is observed that using HCC in the joint reign increased the shear strength and energy dissipation of the beam column joint. Jae-Hoon *et al*. (2015) investigated experimentally the behavior of exterior BCJ using replacing recycled coarse aggregate with hybrid fiber (steel fiber+PVA fiber) in the joint regions under cyclic loading. The results demonstrated that retrofitting the BCJ by using such retrofitting materials enhanced the load carrying capacity of and stabled the failure mode due to the bridge of retrofitting hybrid fiber.

In this study, the experimental results for ten BCJ specimens, which were cast using three different types of concrete in the joint region only, are presented to show the degree of enhancement in shear strength of BCJs achieved through the use of high strength concrete as the replacement concrete. Furthermore, finite element modeling (FEM) was carried out to predict the failure load and the behavior of the normal and the hybrid BCJ. The results of this investigation support the notion of the use of SFRC and UHPC as strengthening material for improvement of shear strength of BCJs, leading to the possibility of the use of hybrid concreting in new cast-in-situ and precast construction.

2. Experimental program

The experimental work consisted of casting and testing of ten beam-column joint specimens using normal concrete (NC), steel fiber reinforced concrete (SFRC) and ultra-high performance concrete (UHPC). Furthermore, the uniaxial compressive strength for the three different types of concretes used in the testing, namely normal concrete (NC), steel fiber reinforced concrete (SFRC) and ultra-high performance concrete (UHPC) was investigated.

2.1 Test specimens

Ten specimens of beam-column joint ensemble, whose dimensions are shown in Fig. 1(a) and Fig. 1(b), were used, keeping the cross sectional dimensions of 250×300 mm unchanged for both beam and column. A development length and anchorage detail of beam longitudinal reinforcement was satisfied according to ACI 318-14 to guarantee shear transfer from beam to the joint. All specimens were cast using the same Portland cement concrete mix NC, except for the common intersecting region of the joint for which SFRC and UHPC were used for some of the specimens replacing NC. In addition to variation in joint concrete, diameter of longitudinal steel rebar, 18 mm (Fig. 1(a)) was used as flexural steel and two stirrups or ties were used within the joint for some of the specimens. The shear reinforcement consisted of 8 mm diameter doubled-legged closed stirrups spaced at 75 mm centers and was used in all beams to ensure that the beam segment did not suffer a premature shear failure. Table 1 shows the details of all test specimens. Of the ten specimens, four were cast entirely with NC, four were cast using SFRC in the joint region and two specimens were cast using UHPC as the joint replacement concrete (Fig. 1(c)).

2.2 Mix design and material properties

Three types of concrete were used in casting the specimens of BCJ, which were NC, SFRC, and UHPC. A mixture of two different sizes of steel fibers i.e., hooked end and straight fibers were used in the ratio of 1:1. The hooked-end steel fibers were 0.2 mm diameter, 25 mm long and with a tensile strength of 2500 MPa, while the straight steel fibers had a length of 0.1 mm, 12.5 mm in diameter,

Table 1 Specimen details

Specimen ID	Joint Region Concrete	Main Steel Reinforcement (mm)	Joint Region Ties	Test Method
NC -18D-M	NC	18	No	Monotonic
NC -18D-C			No	Cyclic
NC-S-18D-M			Yes	Monotonic
NC-S-18D-C			Yes	Cyclic
SFRC-18D-M	SFRC		No	Monotonic
SFRC-18D-C			No	Cyclic
SFRC-S-18D-M			Yes	Monotonic
SFRC-S-18D-C			Yes	Cyclic
UHPC -18D-M	UHPC		No	Monotonic
UHPC -18D-C			No	Cyclic

Table 2 Quantities of constituents for producing 1 m^3 of the SFC & NC mixtures

Concrete Type	Cement (kg)	Fine Dune Sand (kg)	Water (kg)	Coarse Aggregate (kg)	Micro Silica (kg)	Smooth Steel fiber (kg)	Hooked end steel fiber (kg)	Plasticizer Glenium (Liter)
SFRC	500	775	165	925	------	35.52	35.52	3.0
UHPC	900	1005	163	-----	220	76.5	76.5	40
NC	350	737.83	191.6	1106.74	------	------	------	0.35

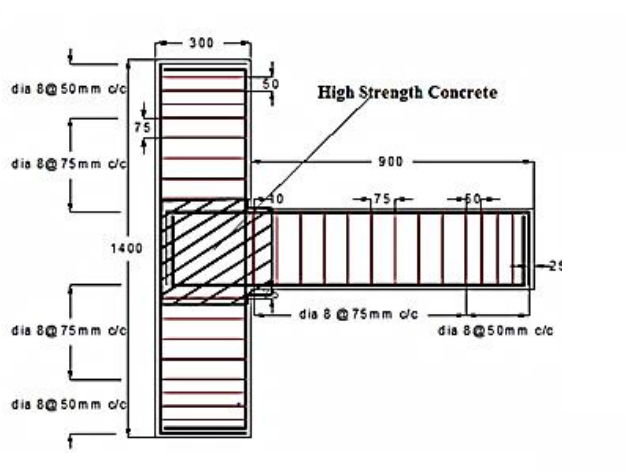

(a) Joint Region without Ties

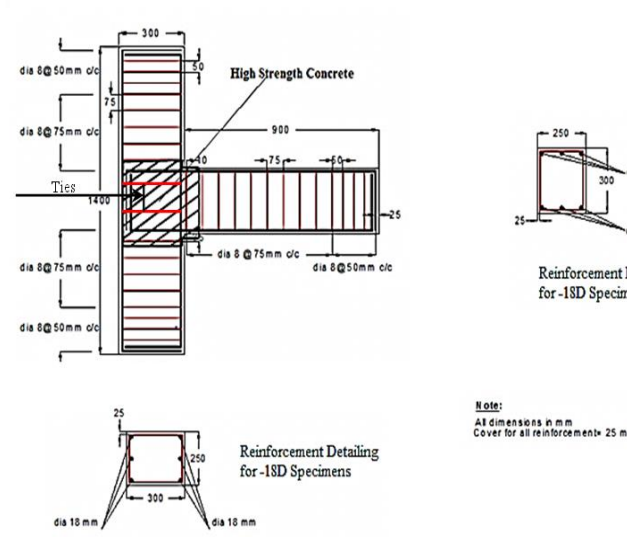

(b) Joint Region with Ties

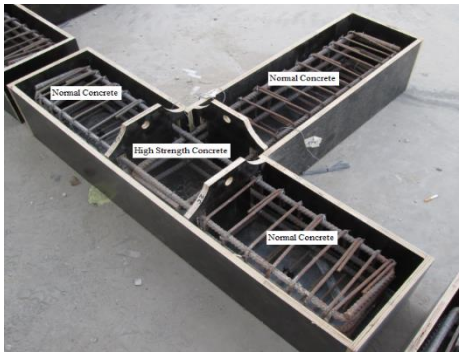

(c) High strength concrete joint

Fig. 1 BCJ specimens' reinforcement details and dimensions

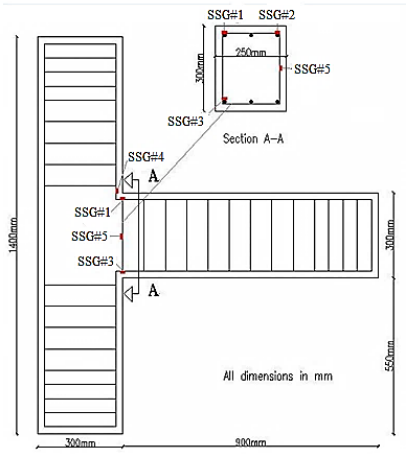

Fig. 2 Strain gauge locations

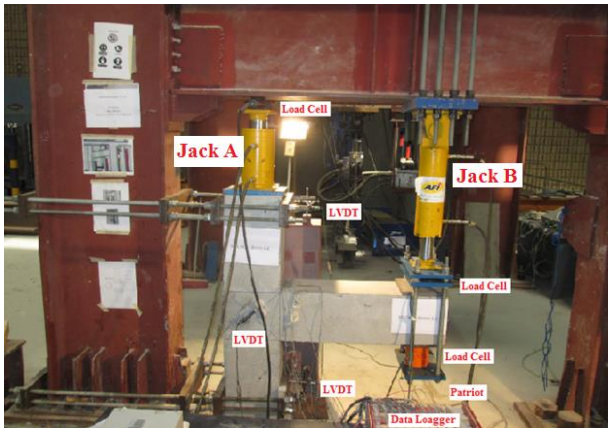

Fig. 3 Instruments used in testing the specimen of BCJ

Fig. 4 Load applied on BCJ specimen

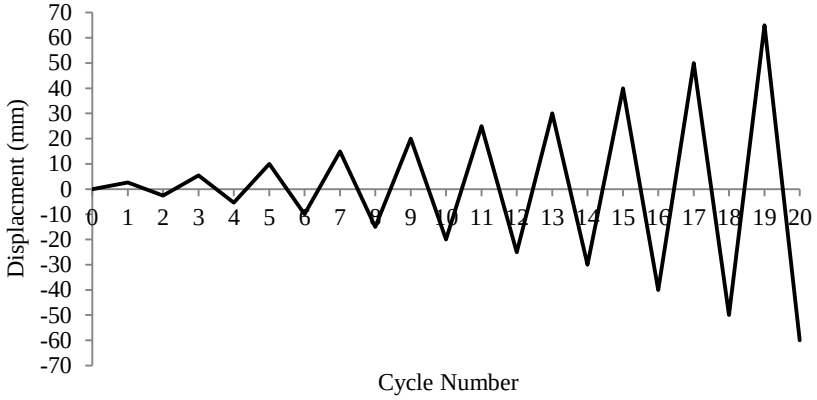

Fig. 5 Loading protocol

and a tensile strength of 2500MPa. The steel fibers were used in the mix design of SFRC and UHPC to enhance the tensile strength of the concrete and hence the shear capacity of the joint region. As the use of steel fiber in a mix reduces the workability of concrete, a dosage of super plasticizer was added to the mix. The mix design for different types of concrete is shown in Table 2.

The compressive strength was determined from testing 75×150 mm cylinders in accordance with ASTM C39. The mean values of compressive strength of the NC was 30 MPa, while for SFRC and UHPC the compressive strength was determined to be 53 MPa and 108 MPa, respectively. Splitting tensile strength was conducted by testing UHPC cylinders according to ASTM C496 to determine the tensile strength of UHPC. The average splitting tensile strength was 7.36 MPa. Similarly, the uniaxial tensile behavior of UHPC was obtained from testing dog bone specimens having a square cross section of dimensions 40×40 mm. The mean values of tensile strength were 11 MPa.

From stress-strain plots of reinforcing bars, the yield strength f_y and the ultimate strength f_u were as follows: for 18 mm diameter bar, f_y=593 MPa and f_u=720 MPa; for 8 mm diameter bar, f_y=568 MPa and f_u=689 MPa.

2.3 Casting and curing of specimens

Prior to casting, five strain gauges were attached to the steel cage of each BCJ specimen as shown in Fig. 2. Water proof plaster was used to protect the strain gauges during the casting process. The prepared steel cage for a specimen was installed in a plywood mold. The reinforcement cover was secured with plastic spacers. The joint area was separated by partitions in order to cast the joint intersection region with high strength concrete and to cast the rest of the specimen using NC (Fig. 1(c)). The partitions were removed before placing SFRC or UHPC. The consolidation of concrete was secured by vibration. The exposed surface of concrete was troweled smooth and then, the specimens were moist-cured for 28 days.

2.4 Test setup and testing of specimens

For testing, the column of the BCJ ensemble was well secured in a vertical position under a test frame. The support system ensured the stability of the test specimens during testing. Two LVDT's were installed at the top and bottom of the column to monitor rotation, and two LVDTs were attached to the intersection area to measure the diagonal crack openings (Fig. 3). The beam deflection was monitored by a string type LVDT. The strain in concrete was measured by attaching strain gauges to the surface of concrete. Each specimen was subjected to two loads applied by hydraulic jacks through load cells, one a constant axial load of 150 kN applied to the column head and the other one a displacement-controlled transverse load P on top of the beam at the cantilever end imposed through controlled displacement of the beam end (Fig. 4). The load on the beam was monotonically increased until the failure load was reached. At each step of beam loading, the test data were recorded by a data logger and the specimen was visually inspected for crack development and advancement.

Cyclic load tests were carried out on five specimens of BCJ to simulate the seismic performance of BCJs using SFRC and UHPC as a replacement NC for the BCJ in the joint region. In these tests, a constant axial load with value of 150 kN was applied first on the top of column then an increasing displacement was applied at the tip of the beam on both push and pull sides up to the failure of the specimen. Fig. 5 shows the loading protocol that was used in the cyclic load test.

3. Numerical Modelling of BCJs

A three-dimensional FEM was created to simulate and predict the behavior and failure load of BCJ specimens by making use of the non-linear finite element package ABAQUS. Dynamic explicit approach was used to overcome convergence problems associated with softening of concrete in tension. The Concrete Damage-Plasticity Model (CDPM) developed by Lubliner *et al*. (1989) and extended by Lee and Fenves (1998) was used to model the nonlinear behavior of NC, SFRC and UHPC while the longitudinal and transverse steel reinforcement was defined as an elastic-plastic material.

Table 3 Concrete parameters used in the plastic damage model

Concrete Strength (MPa)	Mass Density (tonne/mm^3)	Young's Modulus (MPa)	Poisson's Ratio	Dilation Angle ψ (Degrees)	Eccentricity ϵ	f_{bo}/f_{co}	b_c/b_t
Varies*	Varies	Varies*	0.19-0.20	36	0.1	1.16	0.7

*As per concrete strength NC, SFRC and UHPC

3.1 Material models

The nonlinear behavior of the materials was modeled by inputting the CDPM model parameters shown in Table 3. The behavior of the materials in compression of NC, SFRC and UHPC shown in Fig. 6(a), Fig. 6(c) and Fig. 6(e), respectively, was obtained from uniaxial compression test on cylindrical specimens having dimensions of 75 mm×150 mm in a uniaxial compression testing machine. The tensile behavior of NC was obtained by conducing flexural strength test on prism specimens (Fig. 6(b)). However, the tensile behavior of SFRC and UHPC was determined by a direct uniaxial test on dog bone specimens (Fig. 6(d) and Fig. 6(f)).

Concrete compression damage parameters that were used in CDPM model are as given by Birtel and Mark (2006) as

$$d_c = 1 - \frac{\sigma_c E_c^{-1}}{\varepsilon_c^{pl}\left(\frac{1}{b_c} - 1\right) + \sigma_c E_c^{-1}} \quad (1)$$

where: d_c = concrete compresion damage parameter; σ_c = compressive stress; E_c = concrete elastic modulus; ϵ_c^{pl} = plastic strain corresponding to compressive stress; b_c = constant with range $0<b_c<1$.

The concrete tension damage parameter that is used in CDPM model is given by Birtel and Mark (2006) as

$$d_t = 1 - \frac{\sigma_t E_c^{-1}}{\varepsilon_t^{pl}\left(\frac{1}{b_t} - 1\right) + \sigma_t E_c^{-1}} \quad (2)$$

where: d_t = concrete tension damage parameter; σ_t = tensile stress; ϵ_t^{pl} = plastic strain corresponding to tensile stress; b_t = constant with range $0<b_t<1$.

The longitudinal and transverse steel reinforcement behavior was defined as an elastic - plastic material whose parameters were obtained by experimental testing and given by f_y=593 MPa, E=200 GPa (Fig. 7).

3.2 Element types

A 3 - D stress 8 - noded linear brick element (solid continuum) was used to model NC, SFRC and UHPC as shown in Fig. 8.The longitudinal and transverse steel rebars were modeled as 2-noded linear 3 - D truss element, with this element transmitting only axial load. Perfect bond was assumed between concrete and steel rebars.

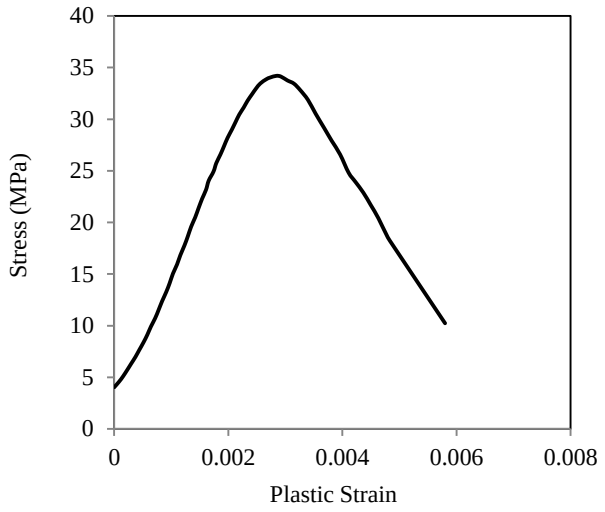

(a)

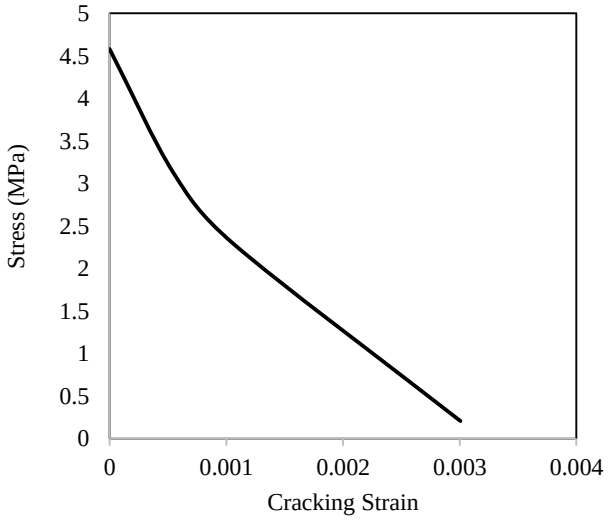

(b)

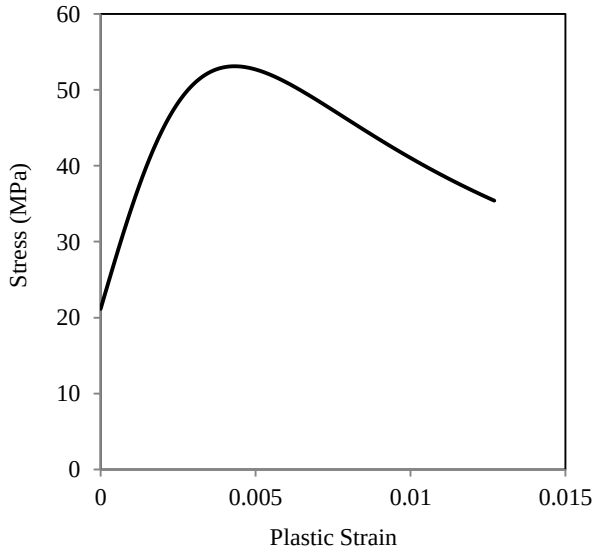

(c)

Fig. 6 Nonlinear behaviour of (a) NC in compression (b) NC in tension(c) SFRC in compression (d) SFRC in tension (e) UHPC in compression (f) UHPC in tension

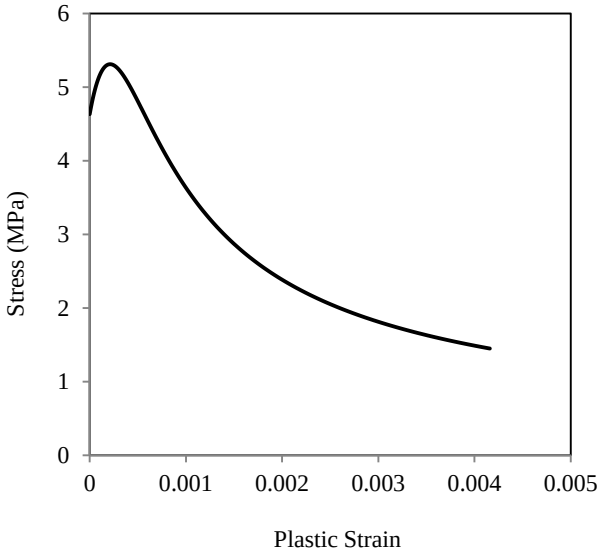

(d)

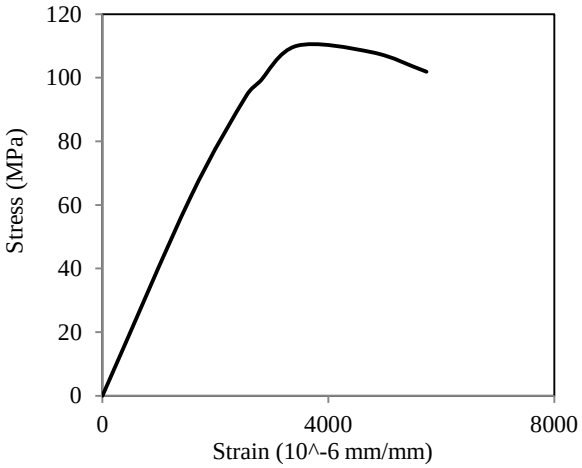

(e)

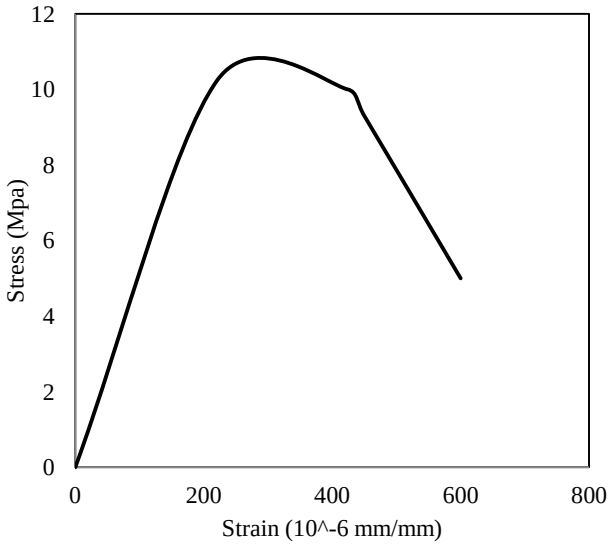

(f)

Fig. 6 Continued

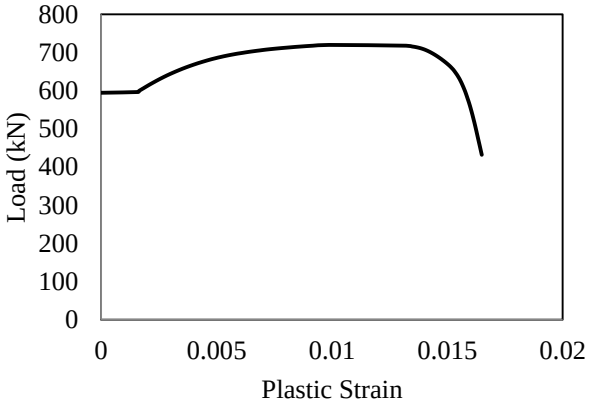

Fig. 7 Behaviour of steel reinforcing bar (18 mm) in tension

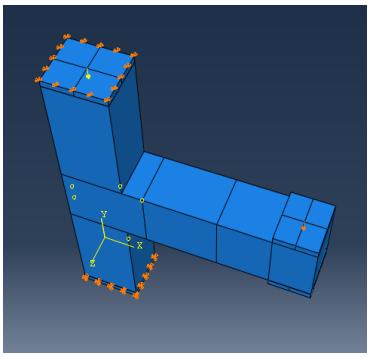

(a)

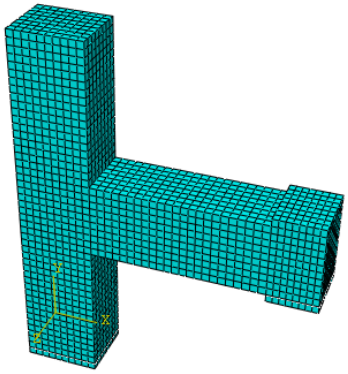

(b)

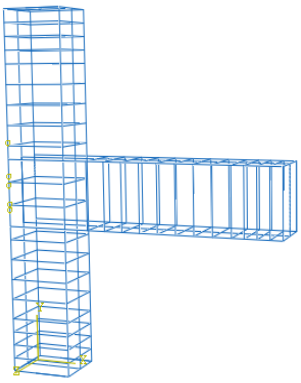

(c)

Fig. 8 (a) Applied loads and boundary condition; (b) Concrete elements and meshing and (c) Steel reinforcing rebars elements

4. Results and discussion

4.1 Ultimate load capacity and mode of failure

The ultimate load capacity, defined as the maximum load P that caused failure, either flexure or joint shear, is shown in Table 4 for all tested specimens, along with the observed mode of failure. Also, shown in Table 4 are the values of P that would cause flexure failure of the cantilevered beam, referred to as P_{uf}. ACI-318-14 building code was used to compute P_{uf} using experimentally determined values of f'_c and f_y. The amount of available strain hardening of reinforcing bars and the limiting concrete strain at failure would result in actual flexural failure load to be greater than the calculated P_{uf} values.

Specimen NC-18D, which was reinforced with 18 mm diameter longitudinal bars, failed in joint shear failure at P_u=97 kN, which was considerably smaller than the load P_{uf} corresponding to the flexural capacity of the beam. The use of two ties within the joint increased the shear strength of the joint for NC-S-18D to 120 kN, an increase of about 25% from the capacity of NC-18D. This improvement however was not sufficient to prevent the joint from failing in shear. The shear failure was confirmed by reading of the strain gauges attached to the top of the beam and found to be less than the yield strain of the reinforcement. The enhancement in shear strength of the joint from the use of SFRC and UHPC as the replacement concrete for the joint can be observed from the P_u values recorded for the specimens. The six specimens, SFRC-18D and UHPC-18D, showed significant improvement in joint shear capacity, resulting in both specimens to fail in flexure. The failure load for all were about the same, being in the range of 150-160 kN. As the failure load P_u was higher than the calculated values of P_{uf} of 135 kN, it appears that actual P_{uf} values were higher due to strain hardening of the steel bars (Fig. 9). The improved shear strength of the joint allowed the beam to carry higher load and resulted in a fundamental change of the failure mode from a brittle joint shear to a ductile flexural failure. More than 50% increase in load capacity was achieved through the strengthening of the joint using high strength concrete as replacement of normal concrete. The specimen SFRC-S-18D did not attain any increase in failure load P_u beyond that of SFRC-18D as the flexure failure of the beam caused failure of the beam-column ensemble. Thus, the enhancement in shear strength due to addition of ties could not be quantified.

As the flexure failure governed the mode of failure for SFRC-18D, SFRC-S-18D and UHPC-18D, the load corresponding to the shear strength of the joint can be surmised to be greater than the experimentally measured P_u values. Therefore, it can be stated that replacement of joint concrete with shear-superior joints allowed attainment of the stated objectives. The experimental data and observations provide further supportive evidence that the shear strength of the BCJ can be enhanced significantly by using high strength concretes like SFRC and UHPC. Their use as the joint-replacement-concrete can be considered as an effective means for strengthening shear strength of BCJs in building and other structures. This idea of hybrid construction may be feasible for frames with slender beam and column sections as per loading requirements, with high joint shear demand requirements. In this case, it may be more cost effective to simply use an appropriate high strength concrete for the joint region only. Such hybrid construction may be applicable for both cast in place and for precast concrete structures.

4.2 Load-deflection plots

In all cases, the load-deflection traces show the familiar plot, with a constant stiffness up to the load causing flexural cracking of the beam, then a gradually decreasing stiffness to the load corresponding to yield moment (Fig. 10 and Fig. 11). Thereafter, specimens other than NC-18D-M/ NC-S-18D-M, showed a sustained post-yielding plastic deformation prior to failure, the amount of which was more than twice the deflection at yield load. The appreciable amount of post-yielding deflection, noted in flexural failure, is a characteristic feature of the sustained ductility of a beam-column joint. For NC-18D-M, in view of the fact that the failure was initiated and dominated by joint shear failure, the post-failure phase was marked by a gradual

Table 4 Failure load and mode of failure test

Specimens #	Failure Load P_u (kN)	Calculated Flexure Failure Load P_{uf} (kN)	Mode of Failure	Test Methods
NC-18D-M	97	135	Joint shear failure	Monotonic
NC-S-18D-M	120	135	Joint shear failure	Monotonic
SFRC-18D-M	156	135	flexural failure	Monotonic
SFRC-S-18D-M	151	135	flexural failure	Monotonic
UHPC-18D-M	160	135	flexural failure	Monotonic
NC-18D-C	99	135	Joint shear failure	Cyclic
NC-S-18D-C	123.4	135	Joint shear failure	Cyclic
SFRC-18D-C	150	135	flexural failure	Cyclic
SFRC-S-18D-C	155	135	flexural failure	Cyclic
UHPC-18D-C	157	135	flexural failure	Cyclic

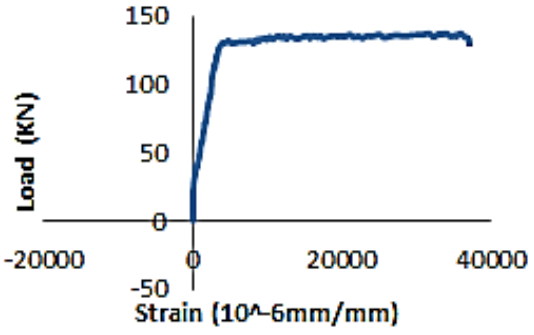

Fig. 9 Load-strain curve for top bar (UHPC-18D-M)

softening until the conclusion of the test as dictated by cracks of large width. The replacement of NC in the joint region with high strength concrete SFRC and UHPC enhanced the shear strength without compromising ductility. Fig. 11 shows a comparison of all BCJ specimens tested under monotonic loading.

Fig. 12 demonstrations the hysteresis response of specimens NC-18D-C, NC-S-18D-C, SFRC-18D-C, SFRC-S-18D-C and UHPC-18D-C. The softening branch was captured in the NC-18D-C specimens, subjected to cyclic loading due to formation of large number of shear cracks in the joint and bond-slip failure between reinforcement and the concrete. The damage of the NC-18D-C specimen was initiated in the beam at the beam-column interface, and then the cracks formed in the joint as the load increased. The specimen failed due to the joint shear damage. The presence of the UHPC and SFRC in the strengthened specimens changed the mode of failure from joint shear failure to the preferred flexural failure. Since the tensile strength of the SFRC is less than the tensile strength of the UHPC, several fine cracks appeared in the SFRC joints. The presence of the ties in the SFRC joint region did not affect the load carrying of the specimen because the main crack was formed in the beam. Nevertheless, the joint region stirrups played a significant role in improving the capacity of NC-S-18D-C specimen.

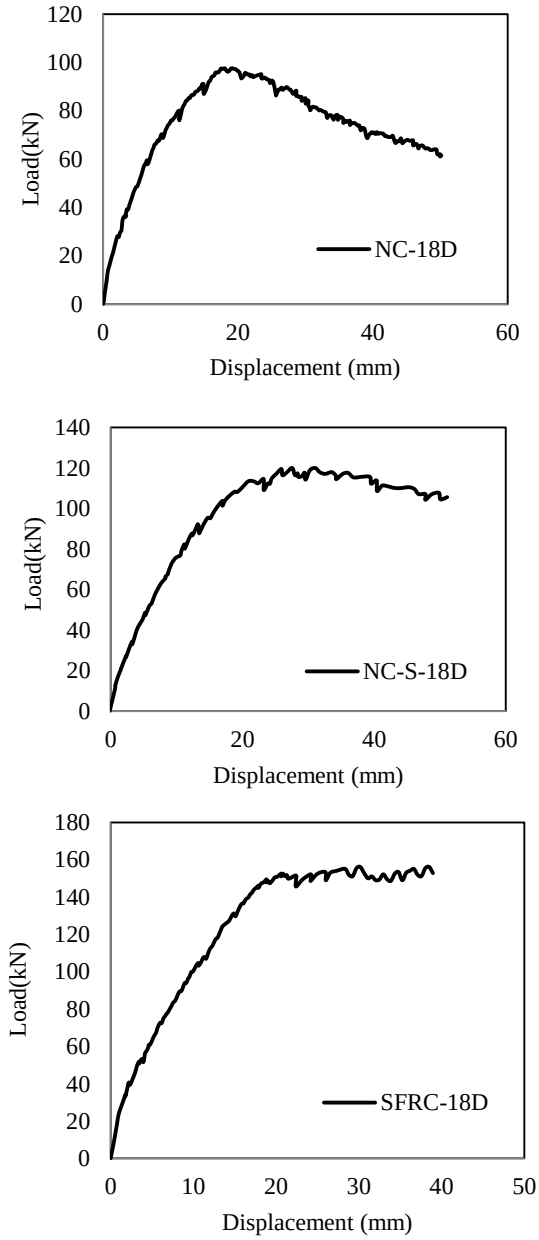

Fig. 10 Load deflection response of BCJ specimens under monotonic loading

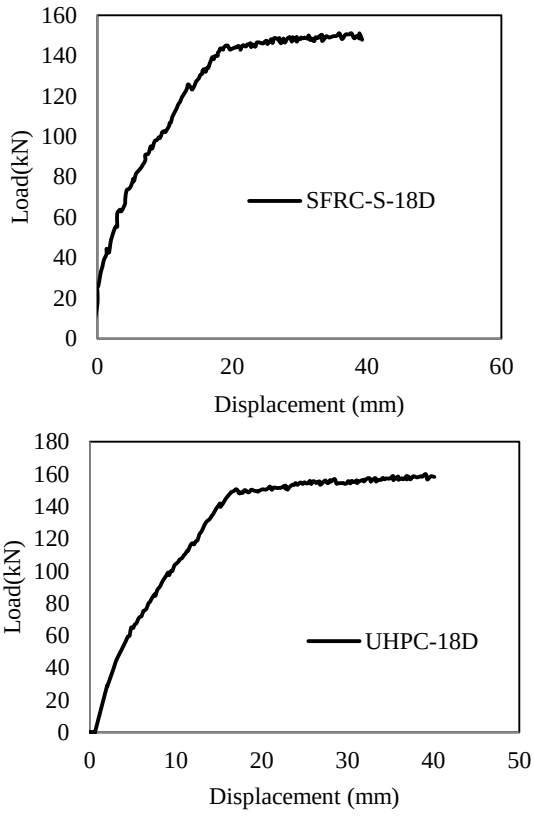

Fig. 10 Continued

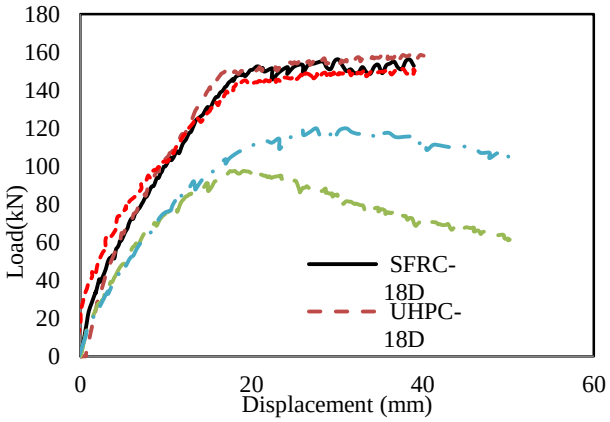

Fig. 11 Comparison of load deflection response of specimens reinforced with 18 mm longitudinal steel bars under monotonic loading

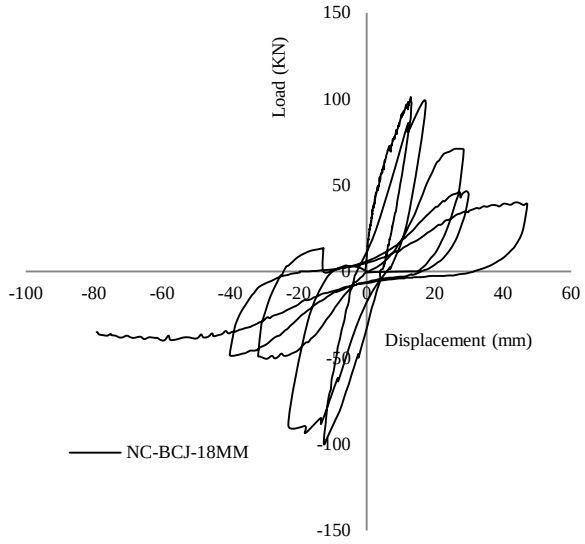

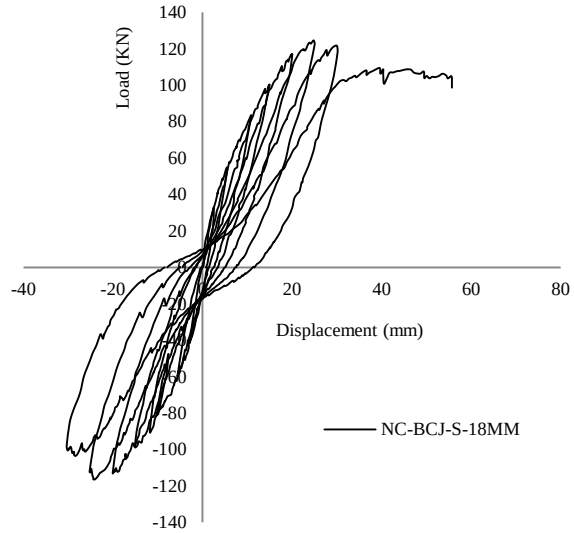

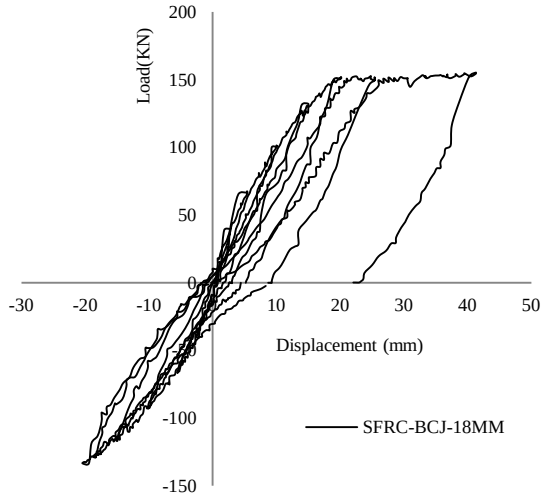

Fig. 12 Hysteresis loop of BCJ specimens

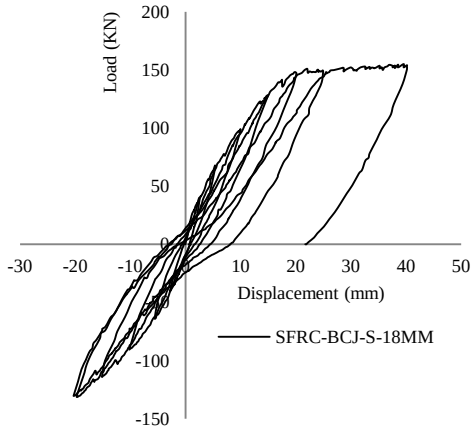

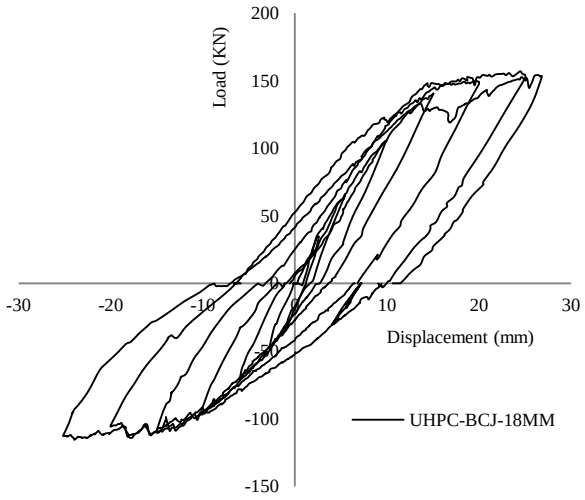

Fig. 12 Continued

4.3 Cracking and mode of failure

The first crack that appeared in the NC-18D specimen was a beam flexural crack, which was followed by several cracks in the beam. Consequently, at a load of 50kN, the first diagonal crack appeared in the joint region. As the load increased, the diagonal crack extended and became wider. The specimen failed due to joint shear failure. This was confirmed by the strain readings in the steel reinforcement, which were recorded as being less than the yield strain. The stirrups in the joint region of NC-S-18D enhanced the load carrying capacity but the appearance of the cracks and the mode of failure remained the same as in NC-18D specimen. The mode of failure of the SFRC-18D, SFRC-S-18D, and UHPC-18D specimens was transformed to that of a beam flexural failure, by virtue of the enhanced shear strength of the SFRC and the UHPC concretes. The first flexural crack in these specimens appeared near the beam-column interface at a load of 40 kN. The cracking load for the admixed concrete specimens was higher than that of the NC specimens, since the joint concrete was also extended into the beam, past the interface region. Due to the high percentage of steel fiber in the UHPC, only one diagonal

fine crack appeared in the joint region of UHPC-18D specimen at load of 146 kN and it remained fine up to the end of the test. However, the first diagonal crack in the SFRC-18D specimen formed at a load of 104 kN followed by several fine diagonal cracks in the joint region. The ties in the joint region of SFRC-S-18D did not affect the behavior of the specimen.

4.4 Shear strength of the joints

Several models are available for prediction of the joint shear strength, Tsonos *et al*. (1993) predicted the joint shear strength based on strut and tie model. The joint shear strength can be computed using the following equation

$$\frac{\alpha\gamma}{2\sqrt{f_{c'}}}\left(1+\sqrt{1+\frac{4}{\alpha^2}}\right)+\frac{5\alpha\gamma}{\sqrt{f_{c'}}}\left(1+\sqrt{1+\frac{4}{\alpha^2}}-1\right)=1 \quad (3)$$

where γ is the joint shear stress expressed as a multiple of $\sqrt{f'c}$, α=h_b/ h_c, h_b is the total depth of beam, h_c is the total depth of column and f_c' is the uniaxial compressive strength of concrete.

Jiuru *et al*. (1992) presented a model to predict the ultimate joint shear strength of fiber reinforced concrete joints based on the assumption that the concrete can resist tensile stress after cracks occur. The ultimate shear strength has three contributions, shear strength resisted by concrete (V_c), shear strength resisted by steel fiber (V_f), and shear strength resisted by joint region stirrups (V_s). These are expressed as

$$V_c = 0.1\left(1+\frac{N}{b_c h_c f_{ac}}\right) b_i h_i f_{ac} \quad (4)$$

$$V_f = 2\frac{l_f}{d_f} v_f b_i h_i \quad (5)$$

$$V_s = f_{ys}\frac{A_{sh}}{s}(d-a_s) \quad (6)$$

where N is the axial compressive load of column, b_c is the width of column, l_f is the length of fiber, v_f is the volume fraction of fibers, b_j is the effective width of joint transverse to the direction of shear, f_{ac} is the axial compressive strength of concrete, f_{ys} is the yield strength of transverse reinforcement, d is the effective depth of beam, S is the spacing of stirrups, a_s is the distance from extreme compressive fiber to the centroid of compressive reinforcement and A_{sh} is the area of shear reinforcement in the joint.

Ilki *et al*. (2011) reported that the joint shear failure is assumed to correspond to the formation of a diagonal crack in the joint. A diagonal crack is assumed to form when principal tensile stress reaches the tensile strength of concrete. The joint shear strength can be expressed as

$$\tau_{vc} = 0.5\sqrt{f_c'}\left(\sqrt{1-\frac{N}{0.5\sqrt{f_c'}A_g}}\right) \quad (7)$$

where A_g is the gross sectional area of the column, N is the axial compressive load of column and f_c' is the uniaxial compressive strength of concrete.

0.5 $\sqrt{f_c'}$ is the concrete tensile strength while Park *et al*. (1997) expressed the tensile strength of the concrete as 0.4 $\sqrt{f_c'}$.

Since Eq. (7) is used often by researchers to estimate the shear strength of beam- column joints, it is of interest to shed further light on the expected variations in the concrete tensile strength and the reasons for such variations.

The stress state in the joint is one of biaxial compression- tension. In a plane stress failure locus, the failure would lie in the fourth quadrant of σ_1-σ_2 space. Using a straight-line approximation, the locus may be represented by

$$\frac{\sigma_1}{f_t}-\frac{\sigma_2}{f_c'}=1 \quad (8)$$

where f_t and f_c' are the uniaxial tensile and compressive strength of concrete.

The loading path to failure may be represented by

$$\sigma_2 = \mu\sigma_1 \quad with \quad -\infty<\mu<0 \quad (9)$$

The column axial load being known, one may compute the vertical stress σ_y with σ_x being zero, the principal stresses can be expressed in terms of the unknown shear stress, v, in the joint at failure e.g., with zero axial load in the column, the ratio μ becomes -1. Substitution of this ratio in Eq. (8) allows for the determination of the principal stress σ_1 and the shear stress at failure i.e., the shear strength of the beam column joint corresponding to a particular level of column axial load. Fig. 13 and Fig. 14 have been drawn using this concept - with the former figure in the 2-D space of column axial stress vs. shear strength of the joint and the latter figure in a similar space, except using σ_y/f_c' and $v/\sqrt{f_c'}$ as the two coordinate axes.

As seen in Fig. 13, the shear strength of the joint is significantly influenced by the axial load on the column. The shear strength increases as the axial load on the column is increased, until a maximum is reached in the range of σ_y between 0.4 to 0.5f_c'. Then the modality of failure changes, similar to the behavior of an axially loaded masonry wall, until the case where the axial stress on the column approaches f_c', the shear strength of the joint reduces to almost zero. Thus depending on the magnitude of the column axial stress, the use of a factor such as 0.5$\sqrt{f_c'}$ for concrete tensile strength (Eq. (7)) may either be conservative (for low axial stress) or may be an incorrect estimate for columns under high axial stress.

This concept illustrates well the dependence of the shear strength of the beam-column joint on the intensity of column axial stress. Most literature on the shear strength of the joint focuses on experiments conducted at a constant level of axial load - and thus this point remains obfuscated from existing literature.

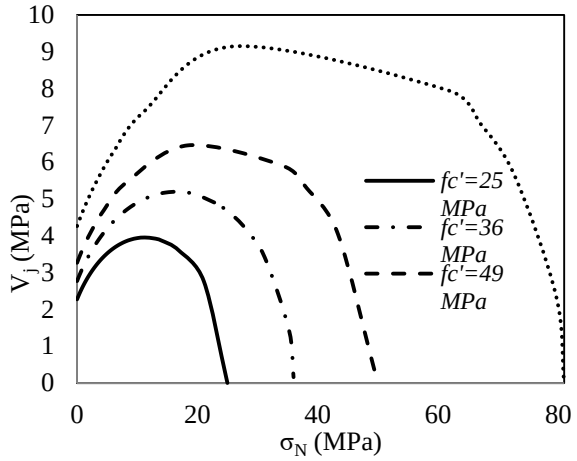

Fig. 13 Plot of column axial stress vs. joint shear strength

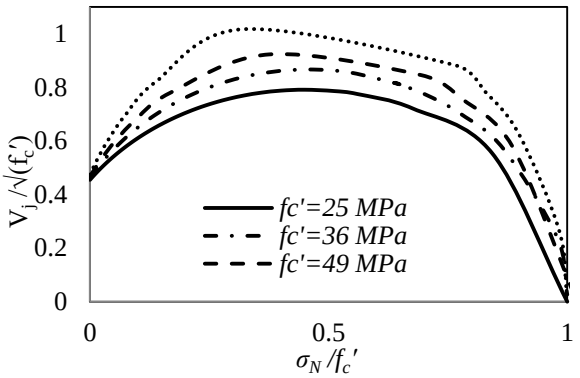

Fig. 14 Plot of normalized of column axial stress vs. joint shear strength

Table 5 Comparison of ultimate joint shear strength

Specimen	Joint Shear at Failure (kN)	V_{th}				
		Ilki *et al*. 2011 (kN)	Park *et al*. 1997 (kN)	ACI-318-14 (kN)	Tsonos *et al*. 1993 (kN)	Jiuru *et al*. 1992 (kN)
NC-18D	241.4	270.2	227.3	511.5	363.1	210
NC-S-18D	304.4	380.5	337.8	622	473.6	320.5
SFRC-18D	428.7	-	-	-	-	480
SFRC-S-18D	417.2	-	-	-	-	590.5
UHPC-18D	404.3	-	-	-	-	795

4.5 ACI empirical equation

An empirical equation is proposed by ACI-318-14 to calculate the joint shear strength of monolithic beam-column joints. The formulation uses a parameter γ, which depends upon the joint type and joint classification. For the case of tested specimens, a value of γ=15 can be used. Using the equations proposed by (Tsonos *et al*. 1993, Jiuru *et al*. 1992, Ilki *et al*. 2011, Park *et al*. 1997), the values of ultimate shear strength were computed and are shown in Table 4 along with the values obtained using the empirical ACI-318-14 expression.

For specimens NC-18-D and NC-18-S-D, it appears that the values of shear strength obtained from the models proposed by (Ilki *et al*. 2011, Park *et al*. 1997) are the closest in comparison to the computed joint shear strength (these BCJ's failed in joint shear) (Table 5). The values of Park *et al*. (1997) are the lowest and the closest to the experimental values for the specimens NC-18-D and NC-18-S-D, both of which were cast with NC and suffered from joint shear strength failure. One of the reasons for the variation in the predicted joint shear strength may well be the role of the axial stress in the column, and how the concrete tensile strength has been estimated. This has been elaborated in the earlier section.

For the SFRC and the UHPC specimens, since the failures were all noted to be flexural, the Jiuru *et al*. (1992) model , which incorporates a component reflecting the contribution of steel fibers to the joint shear strength, yields values of joint shear strength higher than the experimentally determined joint shear force at failure load.

4.6 Experimental joint shear

Using the beam flexural steel strain readings, which were recorded experimentally at the ultimate load P_u, the joint shear force, can be calculated from the following equilibrium equation

$$V_j = T - V_c \tag{10}$$

where T is the total tensile force in main beam reinforcement and V_c is the shear force in the column. The average shear stress in the joint v_{jh} can be computed as

$$v_{jh} = V_j / A_j \tag{11}$$

where: A_j is the area of the joint. Further, the major principal stress, σ_1, can then be determined as

$$\sigma_{(\exp)} = -\frac{\sigma_N}{2} + \sqrt{\left(\frac{\sigma_N}{2}\right)^2 + (v_{jh})^2} \tag{12}$$

where σ_N is the column axial stress.

For specimen NC-18D the failure more was joint shear failure (Fig. 15). In this case substituting the calculated magnitude of v_{jh} in Eq. (12) yields the magnitude of the principal stress σ_1 associated with the shear failure of the joint. Table 6 shows σ_1=0.43$\sqrt{fc'}$ for this specimen. However, for the other specimens reported in Table 6, the failure mode was flexural failure for these cases. In this case, the component v_{jh} is just a measure of the average shear stress (and not joint shear strength), leading to the inequality statement regarding the major principal stress, σ_1.

The joint shear strength for the specimens using steel fibers have two contributions, one being the shear strength resisted by steel fiber and the other component being the shear strength resisted by concrete. Using Eqs. (5), (12), the joint shear strength can be written as

$$V_j = \left(\sqrt{\sigma_1 + \sigma_1\sigma_N}\right)A_j + K\left(l_f / d_f\right)v_f A_j \tag{13}$$

where σ_1 is the principal stress at the ultimate load, σ_N is the

column axial stress, A_j is the joint area, l_f/d_f is the aspect ratio of steel fibre, v_f is the steel fibre content by volume of concrete, V_j is the joint shear force (Table 6) and K is a factor that may be calibrated using appropriate experimental data. In the Jiuru *et al*. (1992) model, the factor K is taken as 2. For the SFRC and the UHPC specimens, since the failure was noted to be flexural, appropriate values for K could not be determined.

4.7 Validation of finite element model

The results obtained from FEM described above have been validated with results obtained from the experimental work.

4.7.1 Specimen NC-18D-M

The load deflection response obtained from FEM for specimen NC-18D-M is shown in Fig. 16 along with experimentally obtained curve. Failure load predicted by FEM is 100 kN corresponding to displacement of 15 mm against experimental value of 97 kN at a displacement of 18.5 mm. It can be observed the FEM result matches closely with the experimental result. The joint and beam crack patterns of the specimen from the experiment and FE prediction are noted to be well matched as shown in Fig. 17.

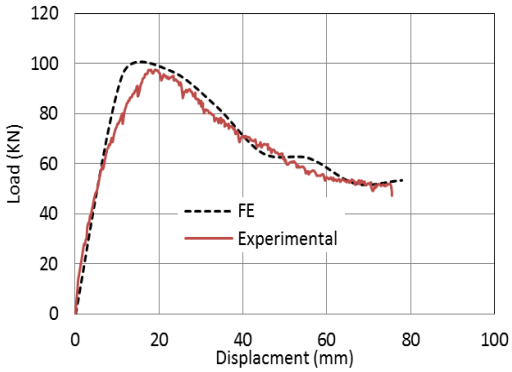

Fig. 16 Load vs. displacement response of specimen NC-18D-M

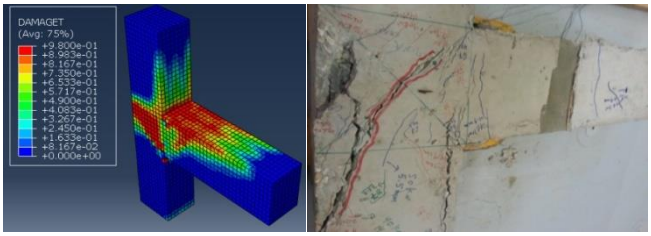

Fig. 17 FEM and experimental crack pattern of specimen NC-18D-M

Table 6 Tensile principal stresses at the ultimate load

Specimen #	NC- 18D	SFRC-18D	UHPC -18D
Ultimate Load (kN)	97	156	160
Mode of Failure	Joint shear failure	Flexure beam failure	Flexure beam failure
ε	0.002	0.005569	0.003839
T (KN)	305.21	529	507.1
V (KN)	241.44	428.71	404.24
v_{jh} (MPa)	3.22	5.72	5.39
σ_1 (MPa)	$0.43\sqrt{fc'}$ f_c' for NC = 30MPa	$\leq 0.79\sqrt{fc'}$ f_c' for SFRC = 53 MPa	$\leq 0.52\sqrt{fc'}$ f_c' for UHPC = 108MPa

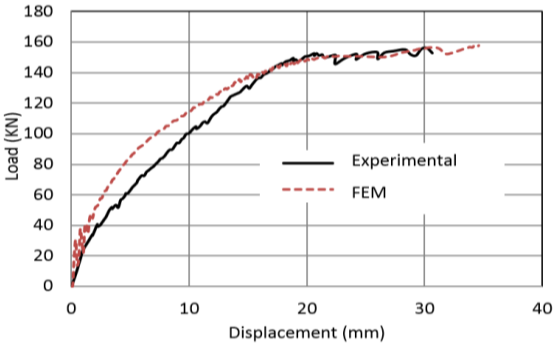

Fig. 18 Load vs. displacement response of specimen SFRC-18D-M

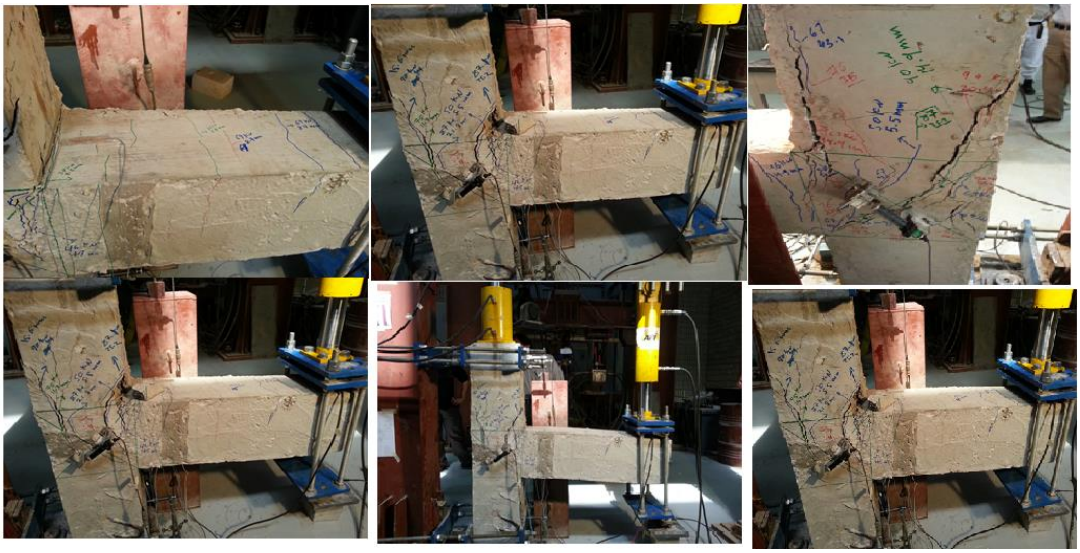

Fig. 15 Crack pattern for specimen NC-BCJ-18MM

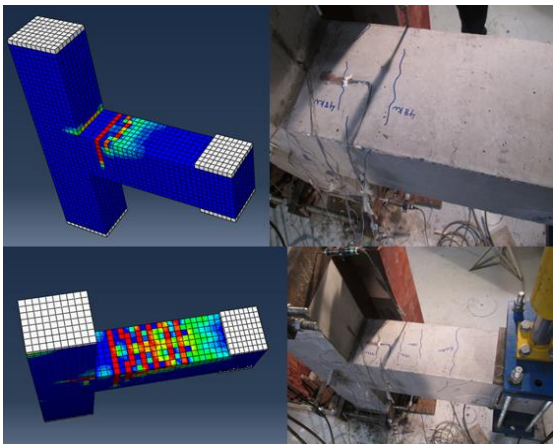

Fig. 19 FEM and experimental crack pattern of specimen SFRC-18D-M

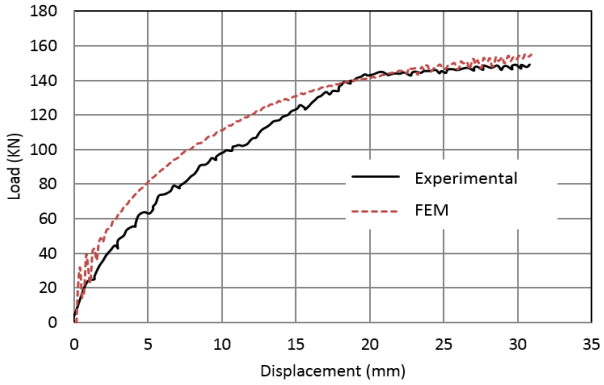

Fig. 20 Load vs. displacement response of specimen SFRC-S-18D-M

4.7.2 Specimen SFRC-18D-M

The load deflection response obtained from FEM for specimen SFRC-18D-M is shown in Fig. 18 along with experimentally obtained curve. Failure load predicted by FEM is 156.5 kN corresponding to displacement of 29.5 mm against experimental value of 156 kN at a displacement of 30 mm. The flexural cracking pattern of specimen from the experiment and FE prediction is noted to match well as shown in Fig. 19Fig. .

4.7.3 Specimen SFRC-S-18D-M

The load deflection response obtained from FEM for specimen SFRC-S-18D-M is shown in Fig. 20 along with experimentally obtained curve. Failure load predicted by FEM is 155.5 kN corresponding to displacement of 30.4 mm against experimental value of 151 kN at a displacement of 30.6 mm.

4.7.4 Specimen UHPC-18D-M

The load deflection response obtained from FEM for specimen UHPC-18D-M is shown in Fig. 21 along with experimentally obtained curve. Failure load predicted by FEM is 160.8 kN corresponding to displacement of 36.22 mm against experimental value of 160 kN at a displacement of 30 mm It can be observed the FEM result closely matches with the experimental result. The mainly flexural

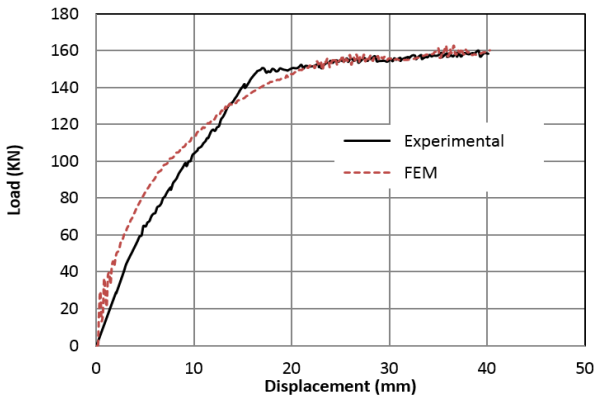

Fig. 21 Load vs. displacement response of specimen UHPC-18D-M

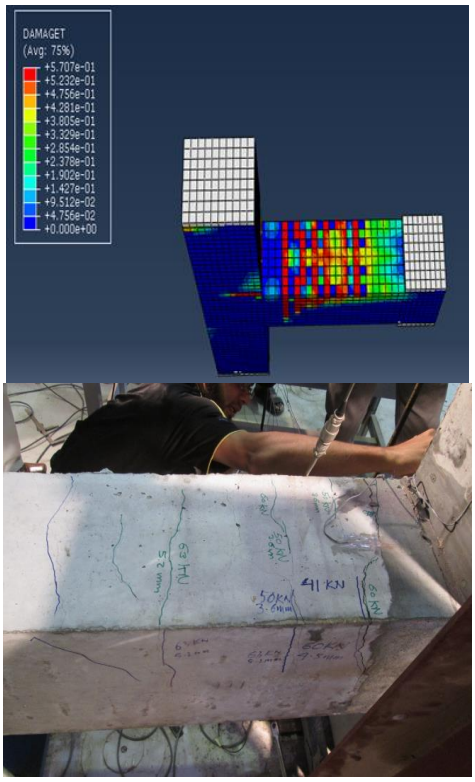

Fig. 22 FEM and experimental crack pattern of specimen UHPC-18D-M

crack pattern of specimen from the experiment and FE prediction appears well matched as shown in Fig. 22.

5. Conclusions

In this study, ten reinforced concrete specimens representing an exterior beam-column joint, cast with variations in joint concrete, were tested to observe the influence of the joint concrete on the shear strength of the joint. Based on the findings of this study, the following conclusions are drawn:

- Both SFRC and UHPC that were used as the replacement concrete for the NC beam-column joints were noted to enhance significantly the shear strength of

the joint and to lead to the preferred flexural mode of failure in contrast to the non-desirable joint shear failure. Such selective replacement provides for a cost effective and innovative method for construction of beam-column joints in frames for both cast-in-place and precast construction that would be shear deficient if cast with normal concrete.

• In some circumstances, SFRC and UHPC joints could also be proposed as a repair and retrofitting strategy for frames with evidence of shear related cracking in the BCJ zone

• The tests have reaffirmed the improvement of shear strength of a beam-column joint through the use of closed reinforcement ties within the confined region of the joint.

• A comparison of the mechanistic models proposed in literature for computation of shear strength of a beam-column joint has shown that the models yield wide-ranging values for the shear strength.

• For a fixed magnitude of column axial stress, the results have shown that the beam-column shear strength for the case of normal strength concrete corresponds to the BCJ major principal stress σ_1 of approximately $0.4\sqrt{fc'}$. For SFRC and UHPC, at the same levels of column axial load, σ_1 was noted to be higher. Exact values could not be determined, as the mode of failure was transformed to a flexural failure in presence of the high strength concretes in the joint region.

• A new theoretical idea has been outlined to account for the influence of the magnitude of the column axial load on the shear strength of a beam-column joint. This shows that for columns with low axial stress, the existing expressions in literature for shear strength of beam-column joints are valid. However, for columns with moderate to high axial loads, the expressions will lead to an over estimate of the shear strength of the joints. A new plot relating the shear strength of the joint to the magnitude of column axial load has been presented, requiring only information about the uniaxial compressive strength of concrete in order to estimate the shear strength.

• The results of FEM simulation for representative beam-column joints tested showed good agreement with the experimental results. The FEM predicted the crack patterns and failure loads close to the experimentally observed values.

Acknowledgements

This investigation is part of the research project, 'Study of Steel Fiber Reinforced Concrete Joints for Beam-Columns Under Cyclic Loading', funded by Deanship of Scientific Research, KFUPM Project **IN131052**. Financial support rendered by them is thankfully acknowledged. The support provided by the Department of Civil and Environmental Engineering and the Center for Engineering Research at Research Institute is acknowledged. The authors also acknowledge the support provided by Saudi Ready Mix Company with the casting of the beam-column joint specimens.

References

Alsayed, S., Al-Salloum, Y., Almusallam, T. and Siddiqui, N. (2010), "Seismic response of FRP-Upgraded exterior RC beam-column joints", *J. Compos. Constr.*, **14**(2), 195-208.

Barros, J., Santos, S., Lourento, L. and Gonçalves, D. (2008), "Flexural behaviour of steel fibre reinforced self-compacting concrete laminar structures", *ISISE - Conference.*

Birtel, V. and Mark, P. (2006), "Parameterised finite element modelling of RC beam shear failure", *In 2006 ABAQUS Users, Conference*, 95-108.

Braga, F., Gigliotti, R. and Laterza, M. (2009), "R/C existing structures with smooth reinforcing bars: Experimental behaviour of beam-column joints subject to cyclic lateral loads", *Open Constr. Build. Technol. J.*, **3**(1), 52-67.

Chidambaram, R. and Agarwal, P. (2015), "Seismic behavior of hybrid fiber reinforced cementitious composite beam-column joints", *Mater. Des.*, **86**, 771-781.

Danish A., Baluch, M., K.Rahman, M. and Ilki, A. (2013), "Finite element modeling of seismic performance of low strength concrete exterior beam-column joints", *Seismic Evaluat. Rehabilit. Struct., Geotech., Geol. Earthq. Eng.*, **26**, 221-242.

El-Amoury, T. and Ghobarah, A. (2002), "Seismic rehabilitation of beam-column joint using GFRP sheets", *Eng. Struct.*, **24**(11), 1397-1407.

El-Dieb, A. (2009), "Mechanical, durability and microstructural characteristics of ultra-high-strength self-compacting concrete incorporating steel fibers", *Mater. Des.*, **30**(10), 4286-4292.

Ganesan, N., Indira, P. and Abraham, R. (2007), "Steel fibre reinforced high performance concrete beam-column joints subjected to cyclic loading", *ISET J. Earthq. Technol*, **44**(3-4), 445-456.

Ha, G. and Shin, J. (2013), "Evaluation of seismic performance of high strength reinforced concrete exterior beam-column joints using high ductile fibre-reinforced mortar", *J. Korea Concrete Inst.*, **25**(4), 419-428.

Ha, J.H., Ha, G.J. and Shin, J.H. (2015), "Improvement and seismic performance evaluation of RC exterior beam-column joints using recycled coarse aggregate with hybrid fiber", *J. Korea Inst. Struct. Mainten. Inspect.*, **19**(2), 160-169.

Ilki, A., Bedirhanoglu, I. and Kumbasar, N. (2011), "Behavior of FRP-retrofitted joints built with plain bars and low-strength concrete", *J. Compos. Constr.*, **15**(3), 312-326.

Jiuru, T., Chaobin, H., Kaijian, Y. and Yongcheng, Y. (1992), "Seismic behavior and shear strength of framed joint using steel-fiber reinforced concrete", *J. Struct. Eng.*, **118**(2), 341-358.

Karayannis, C., Chalioris, C.E. and Sirkelis, G. (2008), "Local retrofit of exterior RC beam-column joints using thin RC jackets-An experimental study", *Earthq. Eng. Struct. D.*, **37**(5), 727-746.

Keerthana, J.D. and Reddy, C.S. (2014), "Experimental investigation on hybrid steel fiber reinforced concrete beam-column joints under cyclic loading", *Int. J. Res. Sci. Technol.*, **1**(11), 6-11.

Lee, J. and Fenves, G. (1998), "Plastic-damage model for cyclic loading of concrete structures", *J. Eng. Mech.*, **124**(8), 892-900.

Lubliner, J., Oliver, J., Oller, S. and Oñate, E. (1989), "A plastic-damage model for concrete", *Int. J. Solid. Struct.*, **25**(3), 299-326.

Oinam, R., Choudhury, M. and Laskar, I. (2013), "Experimental study on beam-column joint with fibres under cyclic loading", *IOSR J. Eng.*, **3**(7), 13-23.

Pampanin, S., Calvi, G.M. and Moratti, M. (2002), "Seismic

behavior of RC beam-column joints designed for gravity only", *12th European Conference on Earthquake Engineering*.

Pantelides, C., Clyde, C. and Reaveley, L. (2002), "Rehabilitation of R/C building joints with FRP composites", *12th World Conference on Earthquake Engineering*, Auckland, New Zealand.

Park, P. (1997), "A static force-based procedure for the seismic assessment of existing reinforced concrete moment resisting frames", *Bull. NZ. Nat'l Soc. Earthq. Eng.*, **30**(3), 213-226.

Perumal, P. and Thanukumari, B. (2011), "Behaviour of M60 concrete using fibre cocktail in exterior beam-column joint under reversed cyclic loading", *Asian J. Civ. Eng. (Building and Housing)*, **12**(2), 255-265.

Prem, P., Bharatkumar, B. and Iyer, N. (2012), "Mechanical properties of ultra high performance concrete", *World Acad. Sci., Eng. Technol.*, **6**(8), 676-685.

Röhm, C., Novak, B., Sasmal, S., Karusala, R. and Srinivas, V. (2012), "Behaviour of fibre reinforced beam-column sub-assemblages under reversed cyclic loading", *Constr. Build. Mater.*, **36**, 319-329.

Sarsam, K. and Al-Azzawi, Z. (2010), "Shear capacity of high-strength fiber reinforced concrete beam-column joints", *Eng. Tech. J.*, **28**(6), 1253.

Sasmal, S., Ramanjaneyulu, K., Novak, B., Srinivas, V., Kumar, K., Korkowskib, K., Roehmb, C., Lakshmanana, N. and Iyera, N. (2011), "Seismic retrofitting of nonductile beam-column sub-assemblage using FRP wrapping and steel plate jacketing", *Constr. Build. Mater.*, **25**(1), 175-182.

Shende, A., Pande, A. and Pathan, M. (2012), "Experimental study on steel fiber reinforced concrete for M-40 grade", *Int. Refer. J. Eng. Sci.*, **1**(1), 43-48.

Song, P. and Hwang, S. (2004), "Mechanical properties of high-strength steel fiber-reinforced concrete", *Constr. Build. Mater.*, **18**(9), 669-673.

Wang, Y. and Lee, M. (2007), "Ultra-high strength steel fiber reinforced concrete for strengthening of RC frames", *J. Marine Sci. Technol.*, **15**(3), 210-218.

Tsonos, A., Tegos, I. and Penelis, G. (1993), "Seismic resistance of type 2 exterior beam-column joints reinforced with inclined bars", *ACI Struct. J.*, **89**(1), 3-12.

KT